COMPUTATIONAL CONTINUUM MECHANICS

ВЫЧИСЛИТЕЛЬНАЯ МЕХАНИКА СЛОШНЫХ СРЕД

Computational Continuum Mechanics. 2021. Vol. 14. No. 3. pp. 289-299 DOI: 10.7242/1999-6691/2021.14.3.24

INFLUENCE OF THE GEOMETRY AND CONFIGURATION OF THE SPHERICAL SLIDING LAYER OF THE BRIDGE BEARINGS ON THE WORKABILITY OF THE STRUCTURE

A.A. Adamov[1], A.A. Kamenskikh[2] and V.I. Strukova[2]

[1]*Institute of Continuous Media Mechanics UB RAS, Perm, Russian Federation*
[2]*Perm National Research Polytechnic University, Perm, Russian Federation*

Spherical bearing contact units consist of an upper steel plate with a spherical segment, a lower steel plate and antifriction polymer sliding layers (spherical and flat). Manufacturers produce the units with different positions of the flat and spherical sliding layer relative to the steel plates of the bearing. However, the effect of the antifriction layer position in the contact unit on the deformation behavior of the structure has not yet been evaluated. In this paper, the influence of the spherical sliding layer position relative to the steel structural elements on their frictional interaction is considered. Two variants associated with the position of the spherical antifriction layer are examined: the sliding layer is applied to the spherical steel segment, and it is located in the spherical notch of the lower steel plate. The design of the spherical bearings includes an interlayer made of radiation-modified fluoroplastic F-4 (no filling). The support unit with an interlayer located in the lower steel plate corresponds to the bearing model L-100 manufactured by AlfaTech LLC (Perm). The L-100 bearing is designed for a normative vertical load of 1000 kN. The maximum length and height of the structure are 155 and 54 mm, respectively, and the interlayer thickness is 4 mm. The support unit with an interlayer applied to the spherical segment is modeled with geometrical dimensions similar to those of the L-100. The standard angle of inclination of the antifriction layer end face is 30°. It was found that the detachment of the mating surfaces by more than 2% of the contact area occurs at a standard angle of the sliding layer end face in the case when the layer is applied to the spherical segment. Therefore, the influence of the inclination angle of the antifriction layer end face on the bearing deformation is considered within the framework of this work. The advantages of the spherical bearing classical design were established in a series of numerical experiments: a more uniform distribution of contact parameters over the mating surfaces, a large area of complete adhesion of the mating surfaces, small deformation of the end face of the sliding layer, etc. Based on the obtained results, the angles of inclination of the end face of the sliding layer were determined, which made it possible to achieve optimal distribution of the parameters of contact zones and the deformation characteristics of the bearings with two variants of the antifriction layer positions.

Key words: bridge structures, spherical bearing, geometric configuration, contact, friction, polymeric materials, full-scale and numerical modeling

1. Introduction

Efficient transport connections, the connectivity of territories within the country and with neighboring countries, the creation of modern functional transport and logistics systems are priorities areas for the development of countries around the world [1-4]. A sustainable transport network includes motor roads of different levels, interchanges with multi-level overpasses, bridgeworks and has a significant impact on the economic development of territories [3, 4]. In the Russian Federation, within the framework of the national project "Safe and high-quality roads", the updated data passport of which was approved in 2021, a number of topical issues are being considered for designing new elements of the road network, as well as monitoring and restoring previously created ones. The solution of these issues will allow the formation of modern safe transport systems in the regions of the country [2, 5].

Bridgeworks [2, 6, 7] and their load-bearing elements are among the critical components of transport systems that require constant monitoring of their technical condition. Over the past decades, there has been a steady growth in the number of vehicles and an increase in traffic flow through road junctions and bridgeworks, which significantly increases the load on the load-bearing elements and determines the requirements for the functioning of transport systems [8-10]. It is noted that the main reasons for failure of bridgeworks are the following [9-12]: destruction due to the loss of stability of bridgework elements; rupture of connections of load-bearing structural units; overload of load-bearing elements, and others. Thus, one of the main factors for the loss of efficiency of bridgeworks is the breakdown of critical load-bearing elements, which include expansion joints [13, 14], bearing parts [15-18], bridge spans [18, 19], lifting structures of drawbridges [20], and others.

Email addresses for correspondence: adamov.aa@ya.ru

There are several directions of research related to the improvement of strength, reliability, and durability of elements of transport systems: rationalization and optimization of structures of critical elements and bridges in general [21, 22], new technologies for the creation and restoration of road objects [22-25], the introduction of new materials with improved physical, mechanical and operational properties [26-28], changing the geometry and configuration of bearings [29-33], and so on. At the same time, there is an increased interest in the deformation behavior of bridge bearing structures and other assemblies when they operate under seismic activity [34-36]. It is important to analyze the influence of both the geometry and configuration of bearings on the stress-strain state of the structure [26, 34], and the materials of the elements on the functionality of the units [27, 37]. Most of the problems are solved within the framework of computer engineering, i.e., on computer models using effective numerical methods [16-18, etc.]; studies are based on the finite element method and use modern application packages to implement the tasks. Currently, there are a number of engineering and scientific solutions aimed at optimizing and rationalizing the bearings of bridges [29-33]: the thickness, shape, and position of sliding layers made of antifriction polymeric materials, as well as the geometric design of recesses for lubricant in polymeric layers, introduction in the design of additional elements. Thus, the study of the effect of both geometry and configuration of elements of bridgeworks is relevant, including using modern numerical methods.

This study presents the results of a comparative analysis of the deformation behavior of two geometries of spherical bearings that differ in the position of the sliding layer relative to the load-bearing steel plates. Previously, the influence of the inclination angle of the end face antifriction layer on the contact parameters and deformation behavior of the spherical bearing was established. Thus, at a standard inclination angle of the end face of 30°, a structure with a sliding layer deposited on a spherical steel segment exhibits a zone of divergence of mating surface near the edge of the interlayer. Therefore, here we consider the deformation of bearings of different geometry and configuration: the angle of inclination of the end face of interlayer varies from 0 to 45° with a step of 5°. The study is aimed at identifying qualitative and quantitative patterns of the influence of the angle of end face inclination and the position of the spherical sliding layer on the performance of the structure.

2. Statement of the problem

We analyze the contact interaction through the antifriction polymer layer of the upper spherical element *1* and the lower steel plate *2* (Fig. 1). Two geometries of the spherical bearing are considered: the antifriction layer *3* fills the recess in the lower steel plate (classical design) — model A (Fig. 1*a*); the layer is applied on the spherical segment — model B (Fig. 1*b*).

Spherical bearings with a height of $h = 54$ mm and width of $b = 2b_k = 155$ mm are designed for a standard vertical load of 1000 kN. The thickness of the sliding layer is constant and equal to $h_p = 4$ mm, $l_p = 65$ mm is the distance to the extreme point of the sliding layer on the surface S_K, along which the spherical segment can turn. The standard angle of inclination of the end face of the spherical sliding layer is 30°. The polymer layer is pressed into the steel structural elements. Radiation-modified, unfilled PTFE F-4 is used as a material for the relatively thin spherical sliding layer.

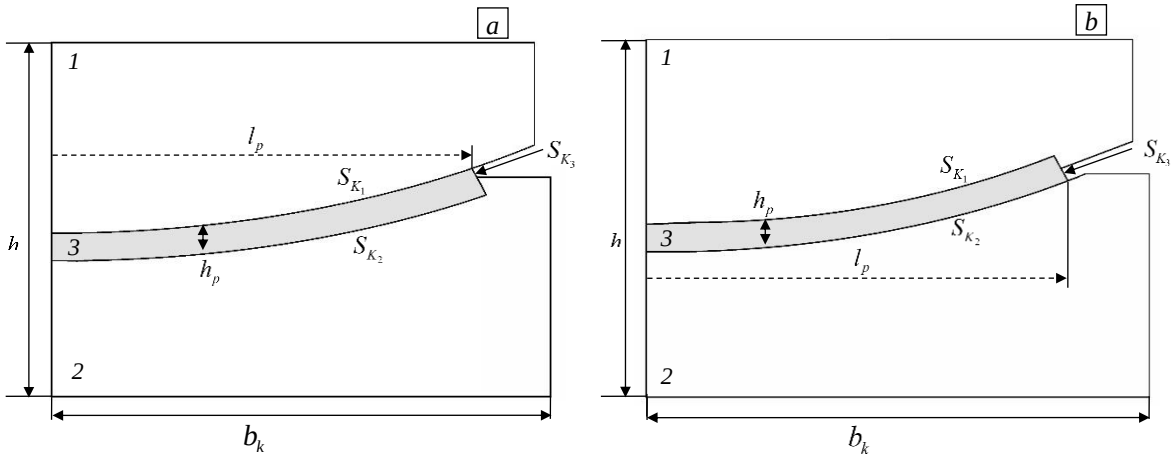

Fig. 1 Calculation diagrams of spherical bearings: model A (*a*); model B (*b*).

The design of the spherical antifriction layer of bridge bearings is of great interest [26] since the sliding layer thickness and the inclination angle of its end face, the position of the layer relative to the steel structural elements, the shape of recesses for the lubricant, and others are important. The geometry of the sliding layer depends on the angle of inclination of the end face α_p (see Fig. 2).

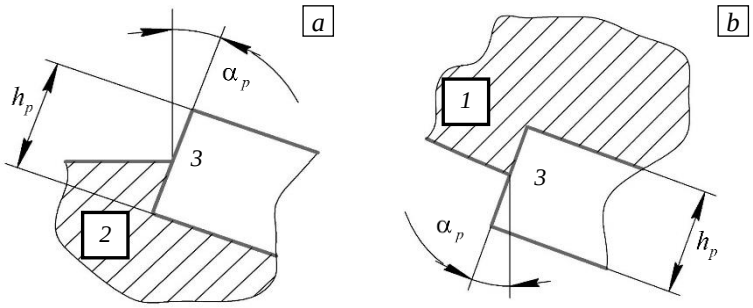

Fig. 2 The geometry of the layer end face: model A (*a*); model B (*b*).

Since, in a comparative study of the deformation behavior of two variants of the structure with different positions of the spherical sliding layer it was found that the standard inclination angle of the end face leads to the appearance of zones of complete "sticking off" of the mating surfaces near the edge of the sliding layer applied to the spherical segment, it was decided to analyze the effect of the end face inclination angle on the structure as a whole, and on the parameters in the contact state zones of the support node elements. We considered 10 values of the inclination angle of the antifriction layer end in the range from 0 to 45° for two configurations of the sliding layer.

The properties of radiation-modified unfilled PTFE F-4 were obtained experimentally, and the deformation theory model of plasticity was chosen to describe its behavior [27]. Its basic physical and mechanical properties are as follows: free compression modulus 863,8 MPa, constrained compression modulus 4235,6 MPa, Poisson's ratio 0,461, friction coefficient on the mating surfaces 0,04 (reference value). The mathematical statement of the problem given in [16] is supplemented by considering large deformations in the volume of the layer material. The statement used here differs from the formulation of this problem by other researchers in that it includes the description and implementation of the frictional contact interaction in the mating zones of the sliding layer with the steel structural elements under the condition of unknown distribution of contact state zones (sticking, sliding, and stripping) in advance.

The standard position of the sliding layer in relation to the steel elements is a spherical notch in the bottom steel plate of the bearing (model A). Therefore, this study compares the deformation behavior of spherical bearing structures at a different location of the sliding layer according to the formula:

$$\Delta X = \left(\left| X_{\text{model A}} - X_{\text{model B}} \right| \Big/ X_{\text{model A}} \right) \cdot 100\%, \qquad (1)$$

where $X_{\text{model A}}$ and $X_{\text{model B}}$ are the values of the compared parameters of models A and B, respectively.

The effect of the inclination angle of the end face of the layer α_p on the deformation behavior of spherical bearing structures was evaluated using the standard value of $\alpha_p = 30°$:

$$\delta X = \left(\left| X\big|_{\alpha_p = 30°} - X\big|_{\alpha_p \neq 30°} \right| \Big/ X\big|_{\alpha_p = 30°} \right) \cdot 100\%, \qquad (2)$$

where $X\big|_{\alpha_p = 30°}$ и $X\big|_{\alpha_p \neq 30°}$ are values of the parameter under study at the standard and non-standard α_p.

The analysis of spherical bridge bearing structures with different sliding layer positions for all variants of the end face inclination angle is conducted in an axisymmetric setting according to the contact parameters of the mating surfaces, displacements along the face normal, and the intensity of plastic strain of the layer. The finite element partitioning of A and B models was chosen according to the results of previous numerical solutions to the problem, which made it possible to reveal the dependence of the implementation accuracy on the degree of discretization of the system. The correlation between the degree of discretization and the accuracy

of the achieved solutions was obtained using the classic example of the geometry and configuration of a spherical bearing [16]. When implementing the problem in the ANSYS Mechanical APDL software package, rectangular four-node elements with Lagrangian approximation (PLANE182) were used, with the aspect ratio close to 1:1. The optimal size of finite elements in terms of polymer layer thickness (side length) was determined to be: 0.25 mm. To discretize the top and bottom plates, a grid of elements was used with a size of 2 times the size of the layer element, 0.5 mm. The study also evaluated the stability of the solution to the problem, including considering the large deformations in the antifriction layer.

3. Analysis of the deformation behavior of elements of spherical bearing

Numerically obtained solutions to the problems of contact deformation behavior of the spherical bearings made it possible to compare the distribution of parameters in the contact state zones at different location of the sliding layer relative to the steel elements (see models A and B), and also to estimate the effect of the sliding layer end face inclination angle α_p on the node stress-strain state.

As an example, Figure 3 shows the distribution of contact pressure and contact tangential stress of the studied models of bearings at a standard inclination angle of the sliding layer end face of 30°. The parameters shown correspond to the contact surface along which the spherical segment can turn — S_{K_1} in model A, S_{K_2} in model B.

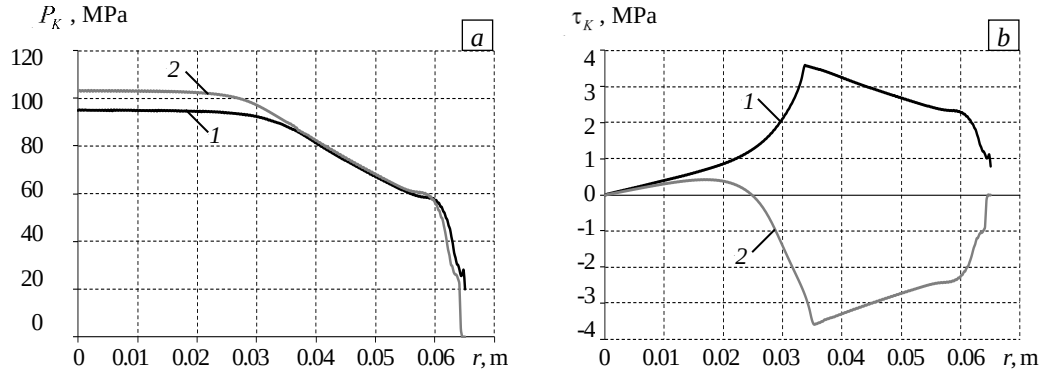

Fig. 3. The pattern of the pressure distribution P_K (*a*) and the tangential stress τ_K (*b*) on the contact surface along which the spherical segment can turn, in model A (curve *1*) and in model B (*2*).

In the two models of spherical bearings under consideration, the pattern of contact pressure distribution has insignificant differences: a small change in the level of P_K near the center of the spherical surface (the zone of full adhesion of the contact surfaces) with a decrease in the contact pressure in the sliding zone. The maximum level of P_K in model B is 8.4% higher than in model A. At the same time, model B has a completely different contact condition near the edge of the sliding layer – the divergence (complete sticking off) of the mating surface by more than 2% of its total area. The pattern of contact tangential stress distribution in models A and B also have differences. Thus, in the zone of change of the contact state from adhesion to slipping, τ_K in Model A increases in the zone of complete adhesion of the contact surfaces and reaches the maximum level, then gradually decreases in the area of slipping; τ_K in model B, it increases by 50% of the area of complete adhesion of the contact surfaces, followed by a sharp decrease in level and smooth growth in the slipping zone. It may be noted that at the standard value of the sliding layer end face inclination angle of 30°, the area of the full adhesion zone in model B is larger than in model A by approximately 10%. According to the results of a series of numerical experiments, the pattern of contact pressure and contact tangential stress distribution is found to have small differences at different angles of the end face inclination. The effect of α_p on the maximum level of contact parameters and their values near the edge of the sliding layer is revealed. Figure 4*a* shows the angle dependence α_p of the $\max P_K$ and $\max \tau_K$ values at the contact surface, along which the spherical segment can turn. The functions $P_K\left(\alpha_p\right)$ and $\tau_K\left(\alpha_p\right)$ near the edge of the sliding layer at $r = l_p$ are shown in Fig. 4*b*.

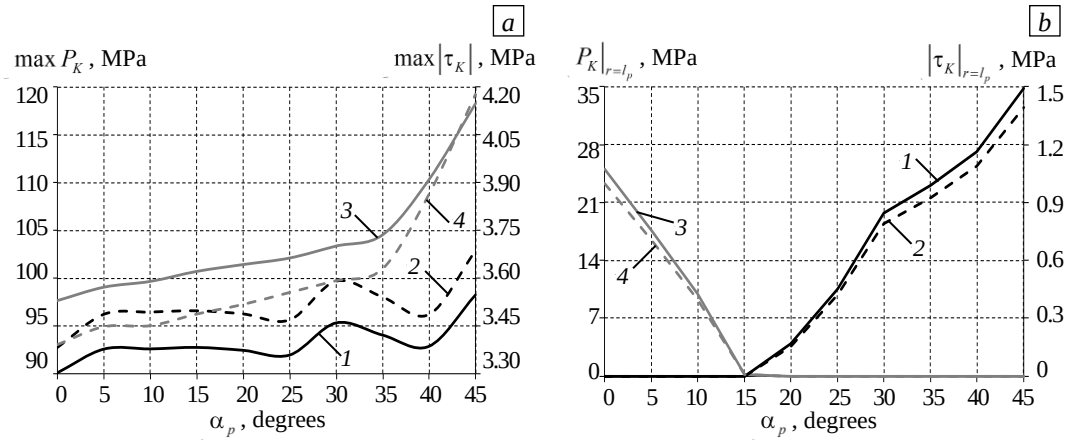

Fig. 4. Dependence on contact parameters α_p: maximum level (*a*); near the edge of the sliding layer at $r = l_p$ (*b*); contact pressure (curves *1*, *3*), contact tangential stress (*2*, *4*); Model A (*1*, *2*) and Model B (*3*, *4*)

The maximum levels of contact pressure and contact tangential stress vary nonlinearly depending on the angle of the end face inclination. The parameters $\max P_K$ and $\max \tau_K$ as functions of α_p in Model B can be described by polynomials of order 4 and higher. Model A at $\alpha_p = 25 \div 40°$ exhibits significant changes in the pattern of curves $\max P_K$ and $\max \tau_K$, which does not allow selecting a mathematical dependence on the sliding layer end face inclination angle for their description. The maximum level of P_K in Model B is greater than in Model A, on average, by 8.7% at end face inclination angles from 0 to 30°; at $\alpha_p > 30°$, the differences of $\max P_K$ between the models increase and reach more than 20% at an angle of inclination of 45°. The contact tangential stress of the models under study at the end face inclination angles from 0 to 35° differ insignificantly, not more than by 2.5%. At the angles of the end face inclination $\alpha_p > 30°$, model B has higher $\max \tau_K$ than model A, at most by 13.3% (at $\alpha_p = 45°$). Near the edge of the sliding layer, a zone of contact surface sticking off appears at a certain α_p: for model A at $\alpha_p = 0 \div 15°$; for model B at $\alpha_p = 20 \div 45°$. Figure 4*b* clearly demonstrates the divergence of mating surfaces near the edge of the sliding layer, which appears in both models, but at different angles of end face inclination. It can be noted that the maximum level of contact pressure and contact tangential stress at the edge of the layer in model A exceeds these parameters in model B by 28%, which corresponds to their more uniform pattern of distribution.

As a result of computational experiments, the effect of α_p on the pattern of distribution of contact states on the mating surfaces (the contact surface along which the spherical segment can turn is of particular interest) has been established. Let us introduce notations: $S_{adhesion}$ is the area that is contact with complete adhesion; $S_{no\ contact}$ is the surface of the sticking off (divergence) of the mating surfaces. Table 1 shows the contact condition on the mating surface for both models of spherical bearings for different models (in percentage of the total mating surface area).

The contact surface area along which the spherical segment can turn and on which the condition of full adhesion applies decreases in most cases with an increase of α_p. It may be noted that the percentage of the mating surface area that is in a state of complete adhesion differs for the two models at most values of α_p. Model A has a higher $S_{adhesion}$ than Model B; the maximum differences in the percentage of the total adhesion area of the mating surfaces are observed at inclination angles of more than 35° and reach 30% or more. The area of the mating surface in the state of complete sticking off is observed for model A at $\alpha_p = 0 \div 15°$ and maximum reaches about 2%, for model B — at $\alpha_p = 20 \div 45°$ and maximum reaches more than 4.5%. The appearance and growth of a zone with complete sticking off on the mating surface has a significant effect on such parameters as S_{K_3} surface displacements along the normal with respect to the free end face of the sliding layer, the intensity of plastic strain, and the maximum level of contact zone parameters.

Table 1. Contact state on the mating surface of different models

Model	Area of contact or unsticking, %	α_p, degrees									
		0	5	10	15	20	25	30	35	40	45
А	$S_{adhesion}$	37.59	32.18	31.11	31.29	31.24	31.43	26.28	27.60	29.51	22.71
	$S_{no\ contact}$	2.23	1.48	1.47	0.74	0.00	0.00	0.00	0.00	0.00	0.00
Б	$S_{adhesion}$	33.07	31.36	31.78	31.36	30.52	29.69	28.87	28.06	22.03	15.78
	$S_{no\ contact}$	0.00	0.00	0.00	0.00	1.49	1.49	2.23	2.97	3.71	4.61

Figure 5*a* shows the pattern of distribution of displacements along the thickness of the anti-friction layer, and Figure 5*b* shows the dependence of their maximum level on α_p.

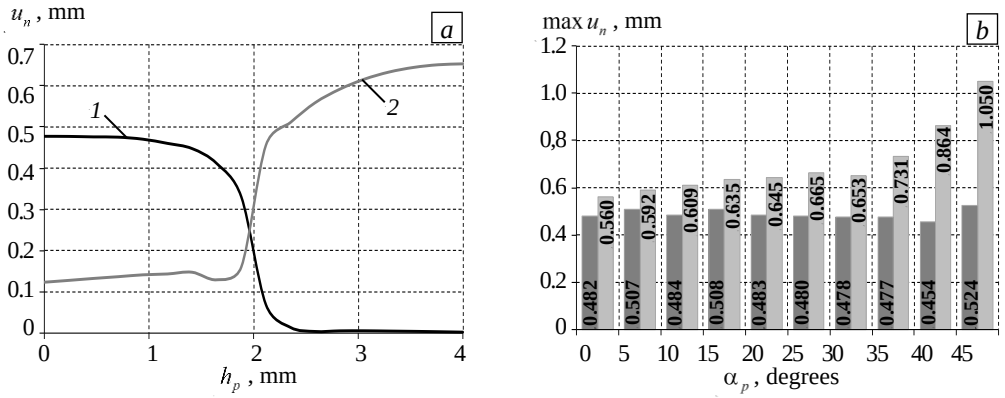

Fig. 5. The pattern of distribution of displacements u_n along the thickness of the layer at $\alpha_p = 30°$ for different models: A (curve *1*); B (*2*) (*a*); dependence of $\max u_n$ on angle α_p (*b*).

The maximum level of displacements along the normal to the surface of the antifriction layer is observed in its relatively free part. At the same time, in model A, in the zone of contact with the steel plate of the sliding layer end face, u_n are close to zero values, which is not characteristic of model B. In the contact zone of the upper steel plate with the end face of the antifriction layer, model B has a normal displacement different from 0, which is associated with a large level of strain and plastic flow of the modified PTFE near the edge of the sliding layer. In general, the pattern of distribution of u_n in the models under consideration in the relatively free part of the end face has small differences, the displacements are maximal near the contact surface of the bearing, along which the spherical segment can turn. Table 2 shows $\Delta \max u_n$, the difference of maximum displacements along the normal to the surface of the bearings of the models at different location of the sliding layer, and $\delta \max u_n$, the estimation of the effect of the end face inclination angle on the maximum displacements S_{K_3}.

Table 2. Effect of the position and inclination angle of the sliding layer face on $\max u_n$

α_p, degrees	0	5	10	15	20	25	30	35	40	45
$\Delta \max u_n$, %	16.22	16.63	25.84	25.16	33.37	38.40	36.71	53.42	90.49	100.25
Model A										
$\delta \max u_n$, %	> 0.88	> 6.18	> 1.33	> 6.26	> 1.19	> 0.54	-	< 0.26	< 5.07	> 9.74
Model B										
$\delta \max u_n$, %	< 14.24	< 9.41	< 6.73	< 2.72	< 1.28	> 1.78	-	> 11.93	> 32.28	> 60.74

When analyzing the data shown in Fig. 5*b* and Table 2, it can be noted that $\max u_n$ for Model B is larger than that for Model A by ~16-100%. The differences in the maximum level of displacements along the normal to the sliding layer end face in both models of bearings considered increase with growth of α_p from 0 to 45°. As a part of the study, a comparison of $\max u_n\big|_{\alpha_p \neq 30°}$ was also made with $\max u_n\big|_{\alpha_p = 30°}$, resulting in the following: at the end face inclination angles different from the standard, model A has differences of the maximum level u_n, but not exceeding 10%; the minimum differences are observed at the face inclination angles of 0, 25 and 35° and are less than 1%; model B at $\alpha_p < 30°$ is characterized by a decrease of $\max u_n$, at $\alpha_p > 30°$ $\max u_n$ has a significant increase, the largest decrease of the maximum level of movements on the normal to the face of the interlayer is observed at $\alpha_p = 0°$ and reaches 14.24%.

The displacements along the normal to the end face relative to the free contact surface of the sliding antifriction layer are related to the manifestation of plastic strain in the polymer material. Figure 6 shows the pattern of plastic strain intensity distribution in the spherical sliding layer for two variants of bearings with a standard end face inclination angle; the enlarged scale shows the zone near the edge of the sliding layer with the maximum level $\varepsilon_{\text{int}_p}$.

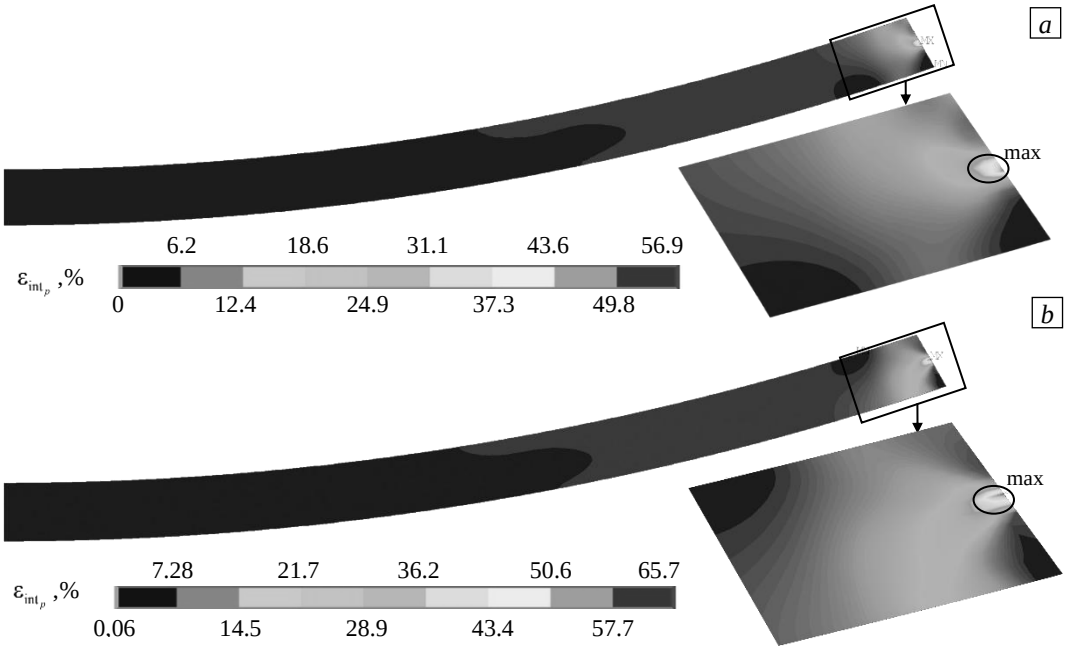

Fig. 6. Pattern of distribution of $\varepsilon_{\text{int}_p}$ at $\alpha_p = 30°$ in different models: A (*a*); B (*b*)

The maximum plastic strain intensity $\varepsilon_{\text{int}_p}$ is observed near the relatively free end of the sliding layer in the mating zone between the steel plate and the antifriction layer. The zone of stress and plastic strain concentration takes place near the beginning of the contact interaction area between the steel plate and the sliding layer. A significant effect of the sliding layer end face inclination angle on the maximum level $\varepsilon_{\text{int}_p}$, distribution pattern, and zone size $\max \varepsilon_{\text{int}_p}$ was found. At the same time, on the most part of the antifriction layer $\varepsilon_{\text{int}_p} < 20\,\%$. It may be noted that $\max \varepsilon_{\text{int}_p}$ of the sliding layer is larger for model B by approximately 15% at the standard end face inclination angle of 30°.

Let us consider the dependence of the maximum level of plastic strain of the spherical antifriction layer on α_p for two variants of the sliding layer position relative to the steel elements of the structure (Fig. 7). As can be seen, for most values, the maximum level α_p of plastic strain in the sliding layer of model B is greater than that of model A. Insignificant differences of $\max \varepsilon_{\text{int}_p}$ are observed for sliding layer end face inclination angles of 5 and 35°. Table 3 shows the differences in the maximum level of strain intensity of the bearings with

different sliding layer positions and provides an estimate of the effect of the end face inclination angle $\max \varepsilon_{\text{int}_p}$ relative to the standard value.

The maximum differences in the level of plastic strain intensity correspond to the end face inclination angles of 20, 25, 40 and 45° and are approximately 50-100%. As part of the study, a comparison of $\max \varepsilon_{\text{int}_p}\big|_{\alpha_p \neq 30°}$ with $\max \varepsilon_{\text{int}_p}\big|_{\alpha_p = 30°}$ was made, which found out that model A has a decrease in the maximum level of plastic strain at the end face sliding layer inclination angles that differ from the standard by more than 30% at α_p, equal to 25 and 40°; model B also has a decrease of $\max \varepsilon_{\text{int}_p}$ at α_p less than 30°, with an increase of α_p>30° at $\max \varepsilon_{\text{int}_p}$. The largest decrease in the maximum level of plastic strain intensity in the spherical sliding layer corresponds to $\alpha_p = 0°$ and reaches 26.5%.

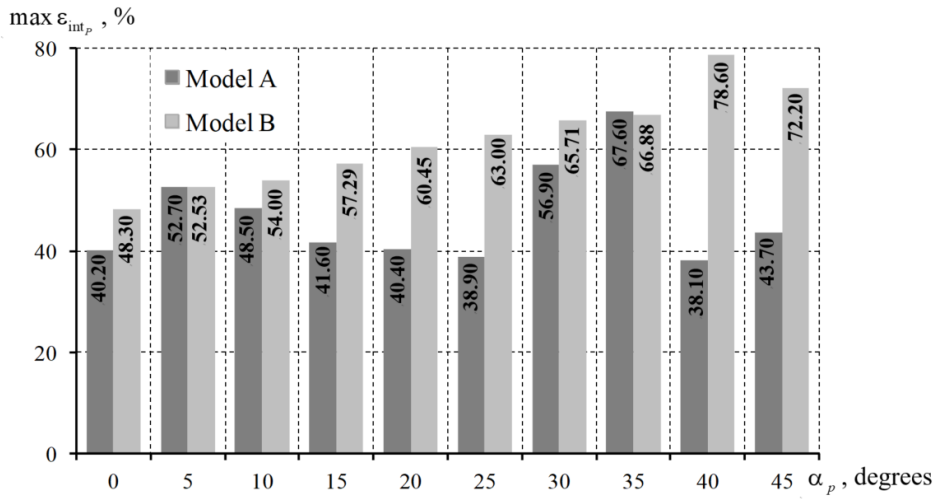

Fig. 7. Dependence $\max \varepsilon_{\text{int}_p}$ on angle α_p.

Table 3. Influence of the position of the sliding layer and the inclination angle of its end on the value of $\max \varepsilon_{\text{int}_p}$

α_p, degrees	0	5	10	15	20	25	30	35	40	45
$\Delta \max \varepsilon_{\text{int}_p}$, %	20.15	0.33	11.34	37.73	49.62	61.95	15.49	1.06	106.30	65.22
Model A										
$\delta \max \varepsilon_{\text{int}_p}$, %	< 29.35	< 7.38	< 14.76	< 26.89	< 29.00	< 31.63	-	> 18.80	< 33.04	< 23.20
Model B										
$\delta \max \varepsilon_{\text{int}_p}$, %	< 26.50	< 20.07	< 17.82	< 12.81	< 8.01	< 4.13	-	> 1.78	> 19.61	> 9.87

The results of numerical simulation of the bearing behavior with a layer filling the bottom steel plate notch are compared with the data of full-scale experiments on the deformation of the classical spherical bearing structure in terms of the settlement value. It has been established that in the axisymmetric setting the error in the results of numerical and full-scale experiments does not exceed 15%. Experimental studies on the deformation of the bearing part with a layer deposited on a spherical segment have not yet been carried out.

4. Conclusion

The analysis of the influence of the angle of inclination of the end face and the location of the sliding layer on the deformation behavior of the spherical bearing parts of the bridge structure has been carried out. Two variants of locating the sliding layer in relation to the steel plates of the bearing: the sliding layer fills a notch in the lower steel plate — Model A; the sliding layer is applied to a spherical segment — Model B. The deformation behavior of Model B is compared with the classical model of the bearing (Model A). The effect of the sliding layer end face inclination angle on the frictional contact of structural elements has been investigated in comparison with the deformation of bearings at a standard 30° end face inclination angle. From numerical experiments, several qualitative and quantitative regularities of the deformation behavior of bridge bearings of different geometry and configuration have been established.

It has been found that the classical position of the spherical sliding layer (Model A) has several advantages: the area of contact surfaces is on average 5% larger than that of model B; when the mating surfaces diverge, the areas in the full sliding state do not exceed 2.5% of their length and appear at the end face inclination angles of less than 20°; the maximum contact pressure and contact tangential stress level are 13 and 20% lower, respectively, than in model B; the displacements relative to the free face of the layer do not exceed 0.55 mm. It has been shown that the most favorable distribution of contact zone parameters and deformation characteristics of the sliding layer is obtained at the end face inclination angles of 25 and 40° for model A and 0° for model B.

The scientific novelty of the results of the study lies in the comparative analysis of the deformation behavior of spherical bridge bearings at different locations of the sliding layer relative to the steel plates of the structure; previously, similar studies have not been carried out.

Computational experiments were performed with axisymmetric setting and deformation of the bearing parts only by the rated vertical load corresponding to the real loads acting on the bearings of bridge spans of a given size. At the same time, in engineering calculations to rationalize the operations on the structure, it is believed that the bearing with the layer applied to the spherical segment will significantly reduce the deformation of the node when additional – horizontal – loads from the bridge span are introduced into the structure. This assumption requires further study in a three-dimensional setting considering different levels and combinations of horizontal and vertical loads.

References

1. Janic' M. *Advanced transport systems*. Springer, 2014. 408 p. https://doi.org/10.1007/978-1-4471-6287-2
2. Reutov E.V., Polozkov A.I. Russian roads: reality and prospects. *Transportnoye delo Rossii – Transport business of Russia*, 2020, no. 2, pp. 201-203.
3. Pryadko I.P. The role of highways in creating a biosphere-compatible urban space: Russian metropolitan experience. *Biosfernaya sovmestimost': chelovek, region, tekhnologii – Biospheric compatibility: human, region, technologies*, 2019, no. 2(26), pp. 111-122. https://doi.org/10.21869/23-11-1518-2019-26-2-111-122
4. Singh S., Martinetti A., Majumdar A., van Dongen L.A.M. (ed.) *Transportation systems: Managing performance through advanced maintenance engineering*. Springer, 2019. 221 p. https://doi.org/10.1007/978-981-32-9323-6
5. Eremin A.V., Volokitina O.A., Volokitin V.P. Management of the condition of bridge structures within the implementation of the national project "Safe and quality car roads". *Vysokiye tekhnologii v stroitel'nom komplekse – High technologies in construction complex*, 2020, no. 1, pp. 12-17.
6. Garcia-Sanchez D., Fernandez-Navamuel A., Sánchez D.Z., Alvear D., Pardo D. Bearing assessment tool for longitudinal bridge performance. *J. Civil. Struct. Health Monit.*, 2020, vol. 10, pp. 1023-1036. https://doi.org/10.1007/s13349-020-00432-1
7. Locke R., Redmond L., Atamturktur S. Techniques for simulating frozen bearing damage in bridge structures for the purpose of drive-by health monitoring. *Dynamics of civil structures*, ed. S. Pakzad. Springer, 2021. Pp. 39-52. https://doi.org/10.1007/978-3-030-47634-2_6
8. Blinkin M., Koncheva E. (ed.) *Transport systems of Russian cities: Ongoing transformations*. Springer, 2016. 299 p. https://doi.org/10.1007/978-3-319-47800-5
9. Ovchinnikov I.I., Maystrenko I.Yu., Ovchinnikov I.G., Uspanov A.M. Failures and collapses of bridge constructions, analysis of their causes. Part 4. *Transportnyye sooruzheniya – Russian Journal of Transport Engineering*, 2018, vol. 5, no. 1, 25 p. http://dx.doi.org/10.15862/05SATS118

10. Proske D. *Bridge collapse frequencies versus failure probabilities*. Springer, 2018. 126 p. https://doi.org/10.1007/978-3-319-73833-8
11. Beben D. *Soil-steel bridges: Design, maintenance and durability*. Springer, 2020. 214 p. https://doi.org/10.1007/978-3-030-34788-8
12. Ye S., Lai X., Bartoli I., Aktan A.E. Technology for condition and performance evaluation of highway bridges. *J. Civil. Struct. Health Monit.*, 2020, vol. 10, pp. 573-594. https://doi.org/10.1007/s13349-020-00403-6
13. Deng Y., Li A. *Structural health monitoring for suspension bridges: Interpretation of field measurements*. Springer, 2019. 243 p. https://doi.org/10.1007/978-981-13-3347-7
14. Okamoto N., Kinoshita T., Futagi T. Development of new embedded expansion joint using high flexibility stone mastic asphalt. *8th RILEM International symposium on testing and characterization of sustainable and innovative bituminous materials*, ed. F. Canestrari, M. Partl. Springer, 2016. Pp. 837-849. https://doi.org/10.1007/978-94-017-7342-3_67
15. Eggert H., Kauschke W. *Structural bearings*. Ernst & Sohn, 2002. 405 p.
16. Kamenskih A.A., Trufanov N.A. Numerical analysis of the stress state of a spherical contact system with an interlayer of antifriction material. *Vychisl. mekh. splosh. sred – Computational Continuum Mechanics*, 2013, vol. 6, no. 1, pp. 54-61. https://doi.org/10.7242/1999-6691/2013.6.1.7
17. Jiang L., He W., Wei B., Wang Z, Li S. The shear pin strength of friction pendulum bearings (FPB) in simply supported railway bridges. *Bull. Earthquake Eng.*, 2019, vol. 17, pp. 6109-6139. https://doi.org/10.1007/s10518-019-00698-x
18. Kuznetsov D.N., Grigorash V.V., Sventikov A.A. Work power of the support unit of the steel I-beam. *Russian Journal of Building Construction and Architecture*, 2021, no. 1(49), pp. 19-29. https://doi.org/10.36622/VSTU.2021.49.1.002
19. Lukin A.O., Suvorov A.A. Bridge spans with corrugated steel webs. *Stroitel'stvo unikal'nykh zdaniy i sooruzheniy – Construction of unique buildings and structures*, 2016, no. 2(41), pp. 45-67.
20. Pozynich K.P., Kligunov E.S. The unbalance problem of the superstructure lifting-transition bridge waterworks. *Dal'niy Vostok: problemy razvitiya arkhitekturno-stroitel'nogo kompleksa*, 2019, vol. 1, no. 1, pp. 326-330.
21. Devitofranceschi A., Paolieri E. Integral bridges: A construction method to minimize maintenance problems. *Proceedings of Italian Concrete Days 2018*, ed. M. di Prisco, M. Menegotto. Springer, 2020. Pp. 515-529. https://doi.org/10.1007/978-3-030-23748-6_40
22. Huang W., Pei M., Liu X., Wei Y. Design and construction of super-long span bridges in China: Review and future perspectives. *Front. Struct. Civ. Eng.*, 2020, vol. 14, pp. 803-838. https://doi.org/10.1007/s11709-020-0644-1
23. Su M., Wang J., Peng H., Cai C.S., Dai G.L. State-of-the-art review of the development and application of bridge rotation construction methods in China. *Sci. China Technol. Sci.*, 2021, vol. 64, pp. 1137-1152. https://doi.org/10.1007/s11431-020-1704-1
24. Kollegger J., Reichenbach S. Balanced lift method – building bridges without formwork. *Proceedings of Italian Concrete Days 2016*, ed. M. di Prisco, M. Menegotto. Springer, 2016. Pp. 200-215. https://doi.org/10.1007/978-3-319-78936-1_15
25. Yu Xm., Chen Dw., Bai Zz. A new method for analysis of sliding cable structures in bridge engineering. *KSCE J. Civ. Eng.*, 2018, vol. 22, pp. 4483-4489. https://doi.org/10.1007/s12205-017-0151-7
26. Adamov A.A., Kamenskih A.A., Pankova A.P. Numerical analysis of the spherical bearing geometric configuration with antifriction layer made of different materials. *Vestnik PNIPU. Mekhanika – PNRPU Mechanics Bulletin*, 2020, no. 4, pp. 15-26. https://doi.org/10.15593/perm.mech/2020.4.02
27. Adamov A.A., Kamenskikh A.A., Nosov Yu.O. Mathematical modeling of modern antifriction polymers behavior. *Prikladnaya matematika i voprosy upravleniya – Applied Mathematics and Control Sciences*, 2019, no. 4, pp. 43-56.
28. Ono K. Structural materials: Metallurgy of bridges. *Metallurgical design and industry*, ed. B. Kaufman, C. Briant. Springer, 2018. Pp. 193-269. https://doi.org/10.1007/978-3-319-93755-7_4
29. Ipanov A.S., Adamov A.A., Patrakov I.M., Kopytov A.V., Kochnev N.V., Tsaplina V.I., RF Patent No. 180825, Byull. Izobret., 26 June 2018.
30. Kopytov A.V., Baltin D.R., Bukanova E.V., Lapin S.N., RF Patent No. 193680, Byull. Izobret., 11 November 2019.
31. Shaferman I.M., Gitman E.M., Shaferman A.I., Rogov A.B., Kopytov A.V., Bukanova E.V., RF Patent No. 194357, Byull. Izobret., 06 December 2019.
32. Shul'man S.A., Slutskaya M.N., RF Patent No. 167994, Byull. Izobret., 16 January 2017.

33. Bukanov V.V., Bukanova E.V., Patrakov I.M., RF Patent No. 181699, Byull. Izobret., 26 July 2018.
34. Khan A.K.M.T.A., Bhuiyan M.A.R., Ali S.B. Seismic responses of a bridge pier isolated by high damping rubber bearing: Effect of rheology modeling. *Int. J. Civ. Eng.*, 2019, vol. 17, pp. 1767-1783. https://doi.org/10.1007/s40999-019-00454-x
35. Zhang Y., Li J., Wang L., Wu H. Study on the seismic performance of different combinations of rubber bearings for continuous beam bridges. *Adv. Civ. Eng.*, 2020, vol. 2020, 8810874. https://doi.org/10.1155/2020/8810874
36. Mahboubi S., Shiravand M.R. Seismic evaluation of bridge bearings based on damage index. *Bull. Earthquake Eng.*, 2019, vol. 17, pp. 4269-4297. https://doi.org/10.1007/s10518-019-00614-3
37. Zhang Y., Li J. Effect of material characteristics of high damping rubber bearings on aseismic behaviors of a two-span simply supported beam bridge. *Advances in Materials Science and Engineering*, 2020, vol. 2020, 9231382. https://doi.org/10.1155/2020/9231382

The authors declare no conflict of interests.
The paper was received on 15.04.2021.
The paper was accepted for publication on 26.06.2021.